CHEMISTRY
A EUROPEAN JOURNAL

DOI: 10.1002/chem.200801624

Density Functional Study of Proline-Catalyzed Intramolecular Baylis–Hillman Reactions

Filipe J. S. Duarte,[a] Eurico J. Cabrita,[a] Gernot Frenking,[b] and A. Gil Santos*[a]

Abstract: The mechanisms of proline-catalyzed and imidazole-co-catalyzed intramolecular Baylis–Hillman reactions have been studied by using density functional theory methods at the B3LYP/6-31G(d,p) level of theory. A polarizable continuum model (PCM B3LYP/6-31++G(d,p)//B3LYP/6-31G-(d,p)) was used to describe solvent effects. Different reaction pathways were investigated, which indicated that water is an important catalyst in the imine/enamine conversion step in the absence of imidazole. When imidazole is used as a co-catalyst, water is still important in the imidazole addition step, but is not present in the Baylis–Hillman cyclization step. The computational data has allowed us to rationalize the experimental outcome of the intramolecular Baylis–Hillman reaction, validating some of the mechanistic steps proposed in the literature, as well as to propose new ones that considerably change and improve our understanding of the full reaction path.

Keywords: asymmetric catalysis · Baylis–Hillman reactions · density functional calculations · reaction mechanisms · transition states

Introduction

Organocatalytic asymmetric reactions are a subject of increasing importance in modern synthetic chemistry,[1] mainly due to the possibility of easy access to important environmentally friendly chiral building blocks. Organocatalysts such as proline, the MacMillan catalyst, the Jørgensen catalyst, or imidazolidinone/oxazolidinone derivatives, have found wide applications in asymmetric Mannich,[2] Michael,[3] aldol,[1b,4] Baylis–Hillman,[5] and Diels–Alder reactions,[6] as well as in the α-amination,[7] α-alkylation,[8] or α-hydroxylation[9] of carbonyl compounds. The β position of α,β-unsaturated aldehydes has also been functionalized, which has allowed the enantioselective conjugated addition of hydride,[10] sulfur,[11] nitrogen,[12] oxygen,[13] and carbon nucleophiles.[14]

The Baylis–Hillman (B–H) reaction allows the direct preparation of highly functionalized β-hydroxycarbonyl derivatives from α,β-unsaturated carbonyl compounds and aldehydes (Scheme 1). The intermolecular version of the B–H reaction has been extensively applied to several different syntheses.[15] The reaction mechanism, specially its achiral form, has also been extensively studied by experimental and theoretical approaches.[16] In contrast, less examples of intramolecular B–H reactions have been reported in the literature,[17] and are mainly based on the cyclization reactions of bifunctional compounds, for example, enone–enone, enone–acrylate, enone–aldehyde, unsaturated thioester–aldehyde,

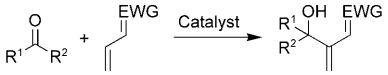

R^1 = aryl, alkyl, heteroaryl; R^2 = H, COOR, alkyl
EWG = electron withdrawing group:
COR, CHO, CN, COOR, $PO(OEt)_2$, SO_2Ph, SO_3Ph, SOPh

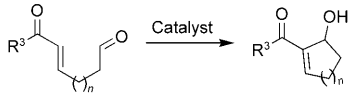

R^3 = Ph, H, OEt, SEt

Scheme 1. Intermolecular[19] and intramolecular Baylis–Hillman reactions.

[a] Dipl.-Chem. F. J. S. Duarte, Prof. Dr. E. J. Cabrita, Prof. Dr. A. G. Santos
REQUIMTE, CQFB, Departamento de Química
Faculdade de Ciências e Tecnologia, Universidade Nova de Lisboa
2829-516 Caparica (Portugal)
Fax: (+351) 212-948-550
E-mail: ags@dq.fct.unl.pt

[b] Prof. Dr. G. Frenking
Fachbereich Chemie, Philipps-Universität Marburg
Hans-Meerwein-Strasse, 35032 Marburg (Germany)

Supporting information for this article is available on the WWW under http://dx.doi.org/10.1002/chem.200801624.

enone–allylic carbonate frameworks. Only a few reports have discussed the mechanistic aspects of intramolecular B–H reactions.[5a,18]

Recently Hong and co-workers[5a] reported the proline-catalyzed enantioselective intramolecular B–H reaction of hept-2-enedial, based on the intermolecular version previously studied by Shi et al.,[20] as affording medium-to-high chemical yields and low optical selectivities. In the presence of imidazole as co-catalyst, the enantioselectivity of the reaction improves considerably and an inverted absolute configuration is observed. The final selectivity, in the presence of a co-catalyst, was observed to be very sensitive to solvent and, to a lesser extent, to temperature. To rationalize the experimental data, Hong and co-workers proposed mechanisms, based on the previous work of Shi et al.,[20] for the enantioselective intramolecular B–H reaction of **1** catalyzed by L-proline in the presence and absence of imidazole

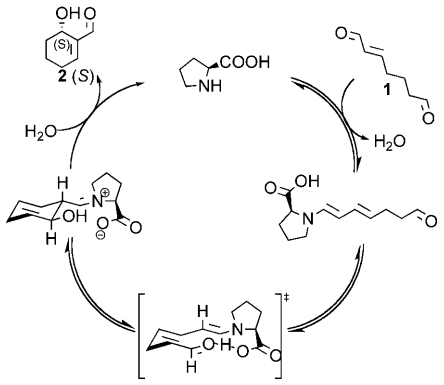

Scheme 2. Proposed mechanism for the L-proline-catalyzed formation of (*S*)-6-hydroxycyclohex-1-enecarbaldehyde ((*S*)-**2**). To simplify the scheme, we considered the direct formation of enamine from the aldehyde.[5a]

(Schemes 2 and 3). The proposed mechanisms involve attack of the enamine intermediate on the free carbonyl group with simultaneous proton transfer from the proline carboxylic acid moiety to the developing alkoxide (Scheme 2). In the presence of imidazole the reaction rate improves and the stereoselectivity reverses (Scheme 3). According to the proposed mechanism, this results from the directed attack of imidazole on the *Si* face of the iminium ion as a result of hydrogen-bond formation between the imidazole iminic nitrogen atom and the carboxylic acid group of the catalyst. The final configuration of the product (*R*)-**2** would result from the configuration adopted in the transition state due to steric interactions between the imidazole ring and the dialdehyde chain.

To the best of our knowledge, no theoretical studies of enantioselective intramolecular Baylis–Hillman reactions have been reported so far. With this work we present the first theoretical study of this type of reaction, the aim being to validate the empirically proposed mechanism or to propose alternatives to explain the experimental data.

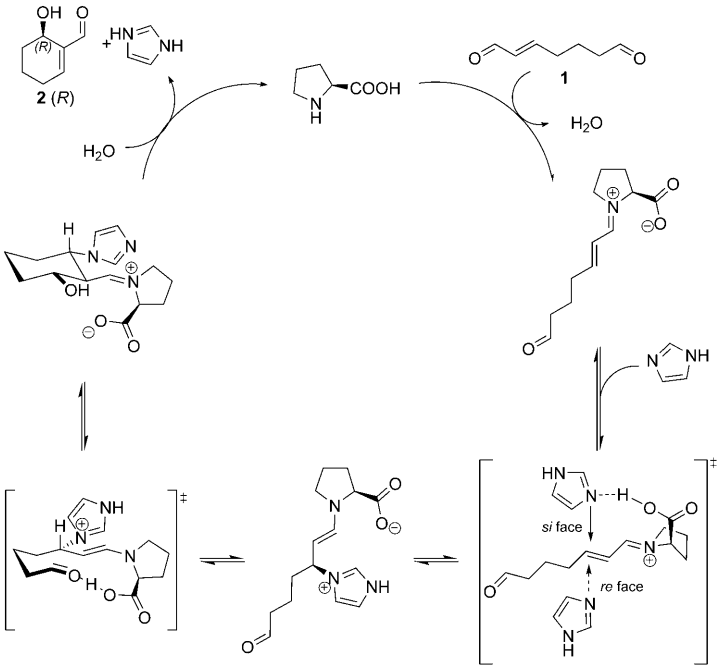

Scheme 3. Proposed mechanism for the L-proline/imidazole co-catalyzed formation of (*R*)-6-hydroxycyclohex-1-enecarbaldehyde ((*R*)-**2**).[5a]

Results and Discussion

The mechanism proposed by Hong and co-workers for the intramolecular B–H reaction of **1** involves attack of an enamine intermediate on the free carbonyl group with a simultaneous proton transfer from the proline carboxylic acid moiety to the developing alkoxide oxygen atom (Scheme 2).[5a] According to Hong and co-workers, inversion of the absolute configuration of the product is observed in the presence of imidazole (Scheme 3). To evaluate the mechanism discussed by Hong, and with the aim of proposing possible alternatives, we first studied the B–H reaction catalyzed by L-proline in the absence of imidazole. The proposed catalytic process is outlined in Scheme 4. As the experimental work was carried out at 25 °C, all the Gibbs' energies given in Scheme 4 were calculated at this temperature.

The first step of the catalytic cycle involves the reaction of the α,β-unsaturated dialdehyde **1** with L-proline to form the corresponding iminium ion with the loss of water. The mechanisms of this step were studied theoretically by Clemente and Houk and are well established.[21] The activation energies are usually low and the reaction is experimentally known to be fast and reversible.[21] Owing to the stereochemistry of the catalyst, two different iminium ions can be formed, each with an *E* configuration and an *anti* or *syn* relationship (Scheme 4; we define the *anti* and *syn* relationships by the relationship between the carboxylic acid group and the carbon chain with respect to the C–N axis).

Our gas-phase calculations show that **3a** (*anti*, *E*) is 4.33 kJ mol^{-1} more stable than its geometric isomer **3b** (*syn*,

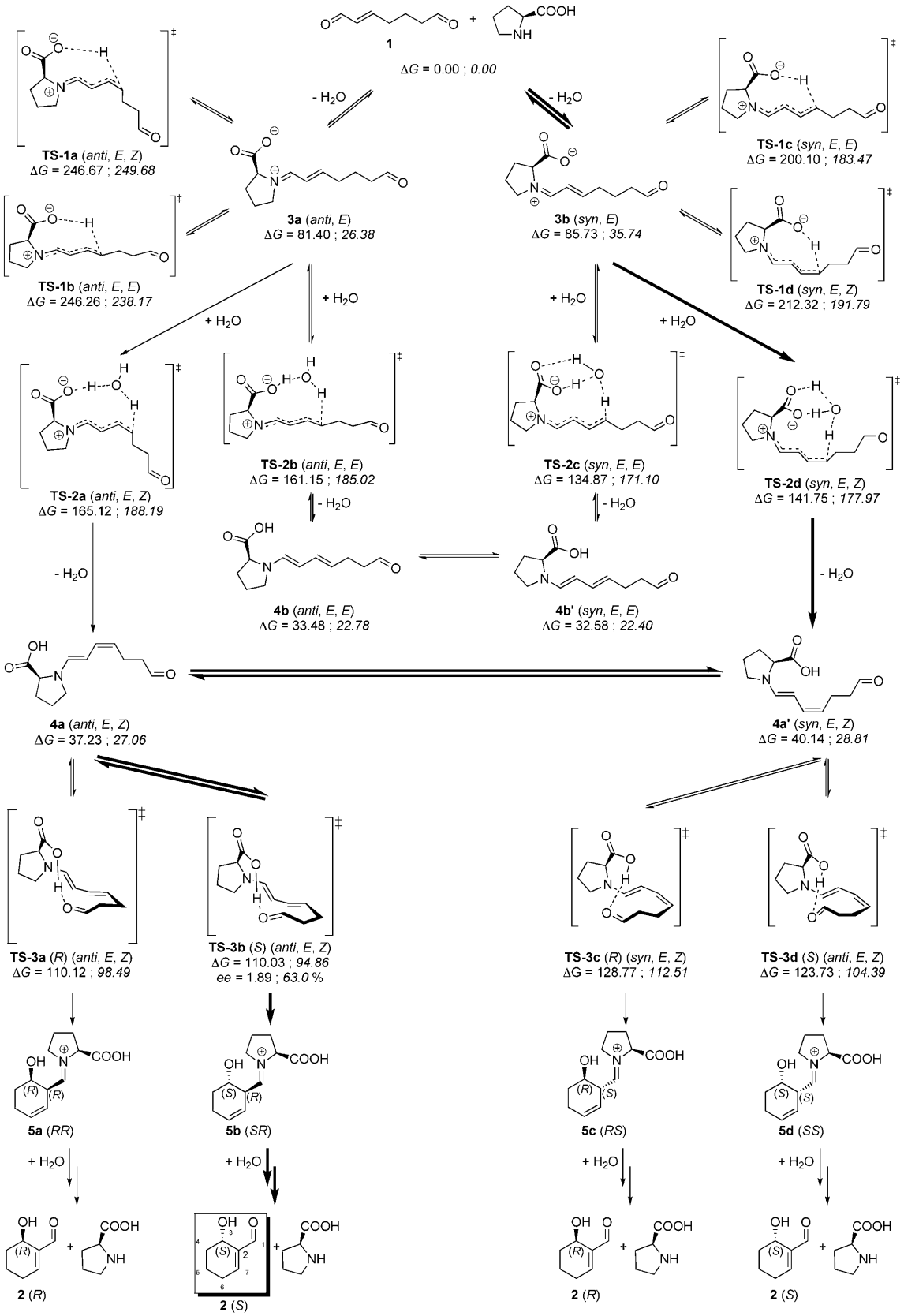

Scheme 4. Proposed catalytic paths, including all intermediates and transition states studied computationally for the L-proline-catalyzed formation of (*S*)-**2**. Free energies (kJ mol^{-1}) calculated at 25 °C at the B3LYP/6-31G(d,p) (plain text) and PCM B3LYP/6-31++G(d,p)//B3LYP/6-31G(d,p) (*italic*) levels of theory. The lowest-energy reaction path is indicated by bold arrows.

E), but the difference increases to 9.36 kJ mol^{-1} in solvent (Scheme 4). The imine intermediate has to convert into the enamine derivative through a deprotononation/protonation step. In saturated systems this interconversion is fast and fully reversible as the prolinecarboxylate is at an appropriate distance to catalyze the transformation, accepting one of the β-protons.[22] However, in this case, the proton has to be removed from the δ position, which is quite distant from the catalytic carboxy group. Our polarizable continuum model (PCM) calculations (Scheme 4 and Figure 1) show that this

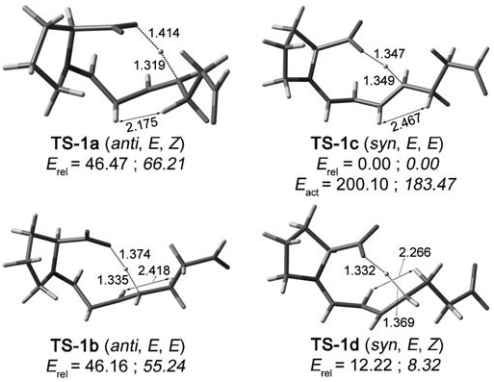

Figure 1. Calculated transition-state structures for the imine/enamine conversion and the relative gas-phase Gibbs' energies at 25 °C (kJ mol^{-1}) at the B3LYP/6-31G(d,p) (plain text) and PCM B3LYP/6-31++G(d,p)//B3LYP/6-31G(d,p) (*italic*) levels of theory.

transformation is associated with high-energy transition states with energies between 183.47 (in **TS-1c**) and 249.68 kJ mol^{-1} (in **TS-1a**) (the values in the gas phase are comparable). The transition-state structures derived from imine **3a** (*anti*, *E*) have the highest activation energies as in this case the distance between the proton to be transferred and the carboxy group is larger. Transition-state structures with a *Z* configuration at both the forming double bonds are not possible as a *Z* configuration at the α,β-double bond implies strong steric contacts between the proline moiety and the carbon chain, which leads to high-energy transition states.

As a water molecule is released during the formation of the imine, an alternative mechanism for enamine formation can be proposed in which water assists the proton transfer. The process can occur through four different transition states, with **TS-2a** and **TS-2b** resulting from the *anti* arrangement of imine **3** and **TS-2c** and **TS-2d** resulting from the *syn* arrangement (Scheme 4 and Figure 2). As discussed previously, *Z* configurations at both forming double bonds are too high in energy and will not be considered.

Because the water molecule is used as a bridge between the carboxy group and the proton at the δ position, the activation energy is substantially reduced ($\Delta\Delta G_{(\mathbf{TS\text{-}1c})-(\mathbf{TS\text{-}2c})}$ = 65.23 kJ mol^{-1} in the gas phase and 12.37 kJ mol^{-1} in solvent) in comparison with the energies of the anhydrous transition-state structures. Transition-state structures **TS-2b** and **TS-2c**

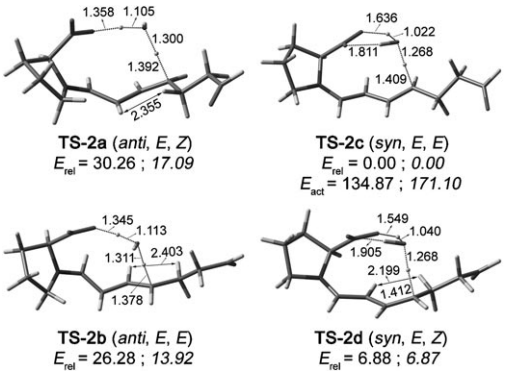

Figure 2. Calculated transition-state structures for water-catalyzed imine/enamine conversion and the relative gas-phase Gibbs' energies at 25 °C (kJ mol^{-1}) at the B3LYP/6-31G(d,p) (plain text) and PCM B3LYP/6-31++G(d,p)//B3LYP/6-31G(d,p) (*italic*) levels of theory.

lead to the enamine with an *E* configuration of the γ,δ-double bond (conformers **4b** and **4b′**). In contrast to the conclusions suggested by the mechanisms of Hong and coworkers, this structure cannot be used in the following B–H cyclization step as the *E* configuration does not allow for a low-energy approach of the reacting functional groups. This implies that the formation of **4b** has to be reversible to justify the yield observed experimentally.

Transition-state structures **TS-2a** and **TS-2d** lead to the enamine with a *Z* configuration at the γ,δ-double bond (conformers **4a** and **4a′**). Nevertheless, as the PCM energy of **TS-2a** is 10.22 kJ mol^{-1} higher than the energy of **TS-2d**, the reaction has to take place through **TS-2d**, originating conformer **4a′**.

Conformers **4a** and **4a′**, with a *Z* configuration at the γ,δ-double bond, can undergo intramolecular B-H cyclization through transition-state structures **TS-3a**–**TS-3d** to afford structures **5a**–**5d** (Scheme 4 and Figure 3). The relative energies of the possible transition states, as well as the calcu-

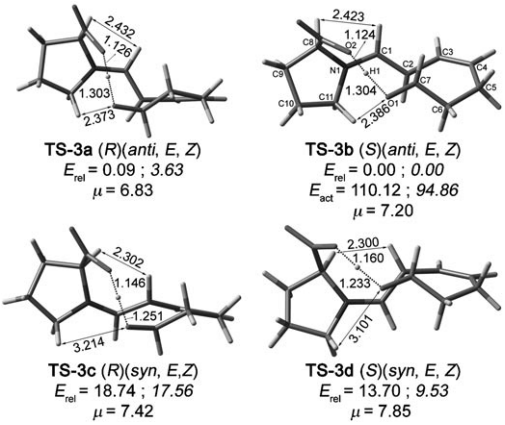

Figure 3. Calculated transition-state structures for the cyclization of **1** into (*S*)-**2** catalyzed by L-proline and the relative gas-phase Gibbs' energies at 25 °C (kJ mol^{-1}) at the B3LYP/6-31G (plain text) and PCM B3LYP/6-31++G(d,p)//B3LYP/6-31G(d,p) (*italic*) levels of theory and dipole moments.

lated selectivities, are given in Table 1. After rearrangement and hydrolysis, structures **5a**–**5d** originate the two possible enantiomers of compound **2**. In conventional intermolecular B-H reactions it is accepted that the rate-determining step (RDS) is usually associated with proton transfer to the formed alkoxylate.[16d–f] Nevertheless, Aggarwal and co-workers[16d] also suggest that in cases in which aliphatic aldehydes are used, the RDS can be the aldehyde addition step. This is suggested to be also the case when activated iminium ions are used instead of the precursor carbonyl groups. In the reaction discussed here, we are dealing with these two situations simultaneously. Also, because of the intramolecular catalytic assistance of the prolinecarboxylate, the product of the aldehyde addition is already an alcohol, which means that there is no need of proton transfer, but only an enamine–imine equilibrium, which is known to be fast and easily catalyzed under the experimental reaction conditions.[21,23] This means that the transition-state structures involved in the conversion of compound **5** to compound **2** will be of low energy and will not account for the overall selectivity. For this reason and also because of the lack of experimental data needed to validate any mechanistic proposal, we will not discuss the conversion of **5** into **2**.

Table 1. Relative transition-state energies, yields, and enantioselectivities of the intramolecular B–H reaction in the gas phase and in acetonitrile.[a]

TS	Gas phase			Acetonitrile			Ref. [5]
	ΔG [kJ mol^{-1}]	Yield [%]	*ee* [%]	ΔG [kJ mol^{-1}]	Yield [%]	*ee* [%]	*ee* [%]
TS-3a (*R*)	0.09	49.03	1.89 (*S*)	3.63 (−11.63)	18.43	63.0 (*S*)	5[b] (*S*)
TS-3b (*S*)	0.00	50.74		0.00 (−15.17)	79.80		15[c] (*S*)
TS-3c (*R*)	18.74	0.03		17.56 (−16.26)	0.0		45[d] (*S*)
TS-3d (*S*)	13.70	0.20		9.53 (−19.34)	1.71		

[a] Gibbs' energy differences are given in brackets: $\Delta\Delta G = \Delta G_{CH3CN} - \Delta G_{GP}$. $E_{act} = G_{\mathbf{TS\text{-}3b}} - G_{\mathbf{reag}}$; E_{act} = 110.03 kJ mol^{-1} in the gas phase and 94.86 kJ mol^{-1} in acetonitrile. [b] In toluene. [c] In acetonitrile. [d] In *N*,*N*-dimethylformamide.

Comparison of the activation energies for the cyclization step (**TS-3**) with the activation energies for the enamine formation (**TS-2**) shows that the former is substantially less energetic, which means that the rate-limiting step has to be the enamine formation (Scheme 4). Thus, as soon as compound **4** is formed, it will react to form compound **5**.

The transition-state structures shown in Figure 3 for the proline-catalyzed cyclization of hept-2-enedial (**1**) are, in many aspects, similar to the model recently proposed by us[22b] and List and co-workers[4d] for the cyclization of heptanedial. The differences arise from the γ,δ-double bond, which was absent in the aldol cyclization of List and co-workers. In all the transition-state structures, the γ,δ-double bond induces the formation of envelope conformations in which the emerging cyclohexane rings have four carbon atoms in the same plane. The aldehyde moiety and its adjacent methylene group are the only groups that can adopt conformations out of the plane, to one or other side, depending on the absolute configurations of the transition states. The hydrogen bond between the carboxylic acid group and the forming alkoxide oxygen acts as an intramolecular acid catalyst (O1···H1···O2, see structure **TS-3b** in Figure 3 for the atom numbering). This type of interaction is well known in enamine-mediated aldol reactions in which the catalyst is proline.[22] In the gas phase the transition-state structure **TS-3b** (the *S* enantiomer) is the most stable, but it is only 0.09 kJ mol^{-1} less energetic than **TS-3a** (the *R* enantiomer). The two transition-state structures **TS-3b** and **TS-3d** originate the same enantiomer ((*S*)-**2**), whereas **TS-3a** and **TS-3c** lead to the enantiomer (*R*)-**2**. In **TS-3a** (*R*) and **TS-3b** (*S*), the carboxylic acid group and the enamine double bond adopt an *anti* relationship with respect to the C-N axis, whereas in **TS-3c** (*R*) and **TS-3d** (*S*) this relationship is *syn*. This conformational difference correlates well with the relative energies of the four transition states (Figure 3 and Scheme 4; in the gas phase, *syn* structures are at least 13.70 kJ mol^{-1} higher in energy than the *anti* structures), which suggests that the calculated energy change is due to the *syn*/*anti* relationship with respect to the C-N axis. Nevertheless, if this is correct, a similar difference should be observed between the energies of structures **4a** and **4a′** (Scheme 4), the precursors of the transition-state structures shown in Figure 3. As a small difference is calculated in this case ($\Delta\Delta G_{(\mathbf{4a'})-(\mathbf{4a})}$ = 2.91 kJ mol^{-1} in the gas phase), another explanation has to be proposed for the large energy difference observed between the *anti* and *syn* transition states in Figure 3.

It is known that the main driving force for the cyclization step is the stabilization of the negative charge on the forming alkoxide group.[22b,24] This means that any attractive electrostatic contact with the O1 atom will contribute to the stabilization of the transition state. A couple of years ago Cannizzaro and Houk demonstrated that α-hydrogen atoms in ammonium ions can establish very strong hydrogen bonds with basic sites.[25] This means that if the nitrogen atom in the proline moiety (Figure 3) becomes positively charged the α-hydrogen atoms are then able to strongly interact with the oxygen atom O1, which reduces the transition-state energy. This is indeed what happens when the transition-state structures are formed as the electronic movement in the direction of the O1 oxygen atom induces a positive charge on the proline nitrogen atom. The interactions between the proline α-methylene group (C11H) and the forming alkoxide moiety (O1) are clearly visible in Figure 3. In the *anti* transition-state structures, these two groups lie at very short distances, which allows for strong electrostatic contacts ($d_{C11H-O1}$ = 2.373 Å in **TS-3a** and $d_{C11H-O1}$ = 2.386 Å in **TS-3b**). In the case of the *syn* structures, these contacts are weaker as the distances between the interacting groups are larger ($d_{C11H-O1}$ = 3.214 Å in **TS-3c** and $d_{C11H-O1}$ = 3.101 Å

in **TS-3d**). The difference in the contact distances of 0.11 Å between **TS-3c** and **TS-3d** justifies the higher activation energy calculated for **TS-3c**. The importance of these interactions can also be observed in the distances between the atoms O2–H1–O1. In the *anti* structures, the H1–O1 distance is larger than in the *syn* structures ($d_{H1-O1}=1.303$ Å in **TS-3a**, 1.304 Å in **TS-3b**, 1.251 Å in **TS-3c**, and 1.233 Å in **TS-3d**) as the negative charge in O1 is more efficiently neutralized by the contact with C11H. The O2–H1 distances follow the opposite trend ($d_{H1-O2}=1.126$ Å in **TS-3a**, 1.124 Å in **TS-3b**, 1.146 Å in **TS-3c**, and 1.160 Å in **TS-3d**). Steric contacts can also contribute to the calculated relative energies, but they are less important. In the *syn* transition-state structures **TS-3c** (*R*) and **TS-3d** (*S*), shorter hydrogen–hydrogen steric contacts are observed between the hydrogen atom at C2 and the hydrogen atom at C8 ($d_{C8H-C1H}=2.302$ Å in **TS-3c** and $d_{C8H-C1H}=2.300$ Å in **TS-3d**) compared with the distances between C1H and C8H in the *anti* conformations **TS-3a** and **TS-3b** ($d_{C8H-C2H}=2.432$ Å in **TS-3a** and $d_{C8H-C2H}=2.423$ Å in **TS-3b** (Figure 3). This difference contributes, to a small extent, to the higher activation energies of the *syn* transition states. The equatorial versus axial conformation of the substituents in the forming ring seems to be less important as **TS-3b** (with the proline moiety in an equatorial position) is only 0.09 kJ mol^{-1} more stable than **TS-3a** (with the proline moiety in an axial position).

The overall results of the gas-phase calculations predict a slight enantiomeric excess of the product (*S*)-**2**, as observed experimentally (Table 1). The experimental work shows that the enantiomeric excess is sensitive to the nature of the solvent, the best results being obtained in polar media.[5a] In agreement with these observations, the results of PCM calculations in acetonitrile (Table 1) predict an improvement in selectivity, with the overall result (63.0%) higher than that experimentally observed (15%). The difference in selectivity calculated in the gas phase and solvent can be attributed to two different types of solvent stabilization. Structures with larger dipole moments are more stabilized in solvent. This means that, due to the relative values of the dipole moments, *syn* structures are more stabilized than *anti* structures and that **TS-3b** is more stabilized than **TS-3a**. On the other hand, solvent effects reduce electrostatic interactions, which increase the activation energies. This effect is larger in *anti* structures as electrostatic attractive interactions are more important than in *syn* structures. In *anti* structures the net effect is a slightly larger stabilization of **TS-3b**, which accounts for the larger calculated enantiomeric excess. The *syn* structures are both stabilized but, due to their relative energies, no net contribution to the final enantiomeric excess is obtained.

As was discussed in the introduction, the addition of imidazole as co-catalyst can improve the yield of the intramolecular B–H reaction but, at the same time, inversion of selectivity is observed. According to Hong and co-workers,[5a] this would result from the attack of imidazole on the *Si* face of the iminium ion directed by hydrogen-bond formation between the imidazole iminic nitrogen atom and the carboxylic acid group of the catalyst (Scheme 3). The final configuration of the product (*R*)-**2** results from the configuration adopted by the transition state because of steric interactions between the imidazole ring and the dialdehyde chain (Scheme 3). With the aim of validating Hong and co-workers' proposal, we performed a full evaluation of the transition states and intermediates involved in the reaction pathway. Based on these results, we have proposed an alternative mechanism, as outlined in Scheme 5. Because the best experimental results with imidazole as co-catalyst were obtained at 0 °C, the energy values shown in Scheme 5 were also calculated at this temperature.

The first divergence from the proposal of Hong and co-workers is related to the nature of the hydrogen-bond formation between the imidazole molecule and the substrate. All attempts to calculate the transition state proposed by Hong failed. The problem is that, according to Hong, the imidazole molecule uses its iminic nitrogen atom to establish a hydrogen bond with the carboxylic group and, simultaneously, the same nitrogen atom attacks the unsaturated chain in a stereocontrolled mechanism (Scheme 3). If such an attack is possible, its activation energy has to be very large as the nitrogen electron-pair is not available for the attack due to ring conjugation. As we have said, all attempts to find this type of transition state failed. We then considered the zwitterionic form of the substrate and attempted to calculate transition states in which the attack of the imidazole would be directed by hydrogen-bond formation between the aminic nitrogen atom and the charged carboxylate group of the substrate. This would leave the iminic nitrogen atom free for the attack on the carbon–carbon double bond. We indeed were able to find this type of transition-state structure, but their PCM energies were very high ($\Delta G=$ 162.88 kJ mol^{-1} for the *anti* structure and $\Delta G=$ 170.53 kJ mol^{-1} for the *syn* structure) compared with other alternatives (discussed below), which means they are unimportant in the following discussion (see additional data in the Supporting Information). Also, energy values as large as these for the imidazole addition step would bring the addition step in direct competition with the imine/enamine conversion step (Scheme 4), which would possibly lead to low final selectivities. The high-energy values calculated result from the strong distortion imposed on the transition-state structures by the relative positions of the two nitrogen atoms in the imadozole ring.

Because the hydrogen atom at the C2 position in the imidazole molecule has a strong acidic character, it can also be used to establish hydrogen bonding with the carboxylate group, which allows controlled selectivity. This mechanism is outlined in Scheme 5 and Figure 4 shows the calculated transition-state structures along with the corresponding relative energies in the gas phase and in acetonitrile at 0 °C.

According to the data in Figure 4, the addition of imidazole yields epimer (*S*)-**6a** as the major isomer. If solvent effects are considered the selectivity is improved. The calculated energy differences between **TS-4a** and **TS-4b** mainly result from the energy differences observed in the iminic

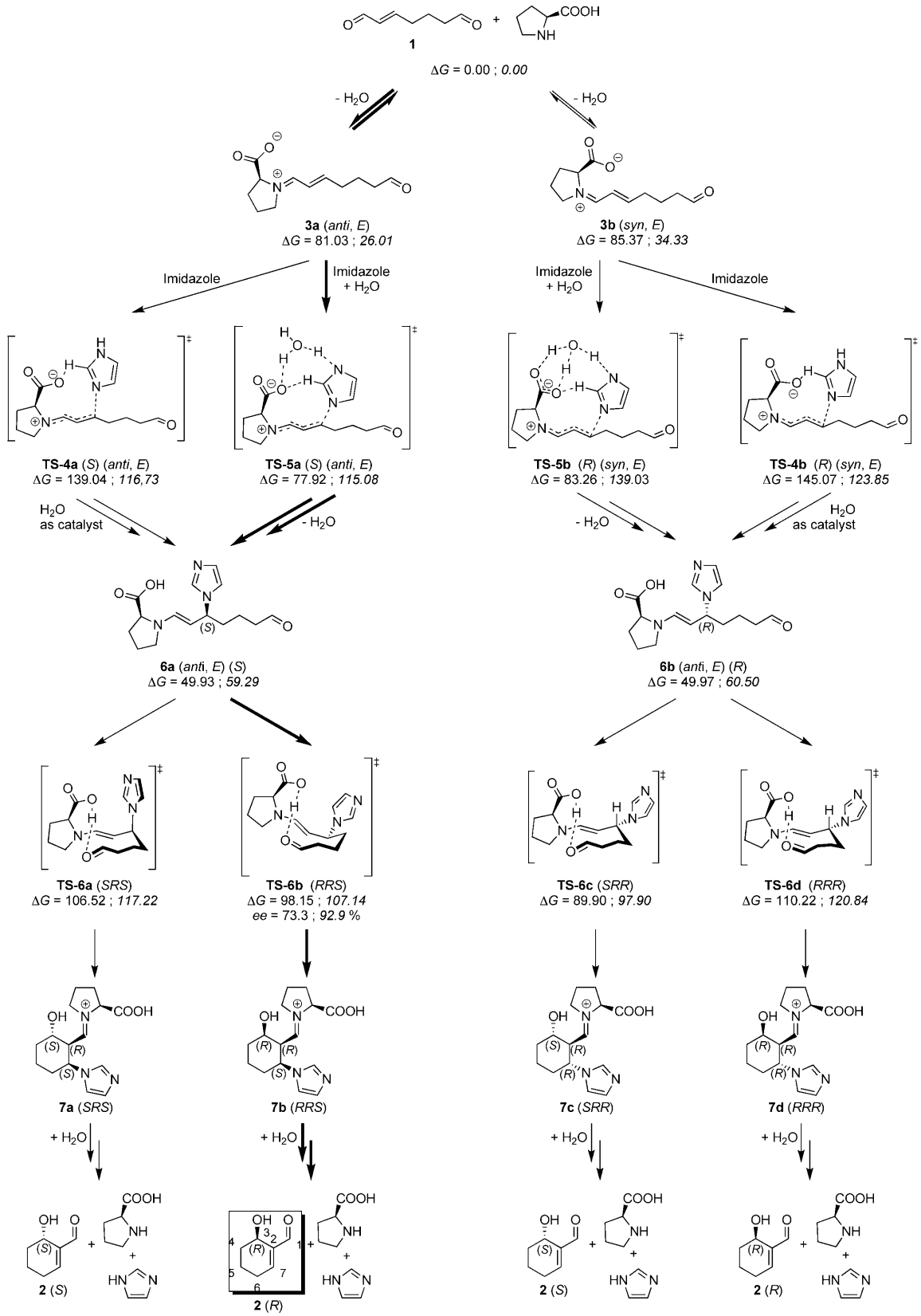

Scheme 5. Proposed catalytic paths with reaction intermediates and transition states studied computationally for the L-proline/imidazole-catalyzed formation of (*R*)-**2**. Free energies (kJ mol^{-1}) calculated at 0 °C at the B3LYP/6-31G(d,p) (plain text) and PCM B3LYP/6-31++G(d,p)//B3LYP/6-31G(d,p) (*italic*) levels of theory. The lowest-energy reaction path is indicated by bold arrows.

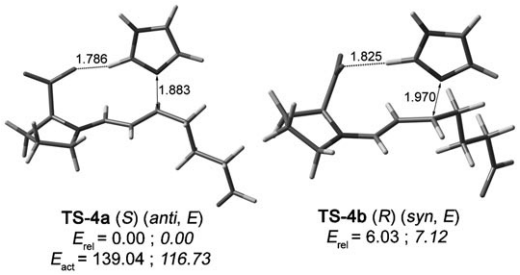

Figure 4. Calculated transition-state structures for the addition of imidazole and the relative gas-phase Gibbs' energies (kJ mol^{-1}) at 0 °C calculated at the B3LYP/6-31G(d,p) (plain text) and PCM B3LYP/6-31++G(d,p)//B3LYP/6-31G(d,p) (*italic*) levels of theory.

precursors. The most stable transition state (**TS-4a**) originates from imine **3a**, whereas transition state **TS-4b** originates from imine **3b**, the *anti*/*syn* energy differences calculated for the imines are similar to those of the transition-state structures.

The two transition states shown in Figure 4 can indeed explain the selective addition of imidazole to originate the *S* epimer, as postulated by Hong and co-workers. Nevertheless, the resulting intermediates, with structures very similar to the previous transitions states, are of high energy (PCM: 93.65 kJ mol^{-1} for the intermediate resulting from **TS-4a** and 102.88 kJ mol^{-1} for the intermediate resulting from **TS-4b**; the structures are not shown in Scheme 5 but are given in the Supporting Information) because the imidazole ring now has a positive charge, which is only partially neutralized by the hydrogen bond with the carboxy moiety. Low-energy intermediates (**6a** and **6b**) can be formed after proton transfer from the imidazole nitrogen atom to the carboxy group and, as this transfer is a simple acid/base reaction, the activation energy should be very low or even zero. Nevertheless, all our attempts to find low-energy transition states for this transformation failed as the distance between the hydrogen atom to be transferred and the carboxy group is too large. The inclusion of a water molecule, a side-product of the imine formation, drastically changes this scenario as it lowers the intermediate energies to values similar to those calculated for structures **6a** and **6b**. This indicates that water, or another acid/base catalyst, are indeed needed for proton transfer between the imidazole moiety and the carboxy group. The scan of the water addition and proton transfer step indicates that this mechanism has no measurable activation energy and, for this reason, it is not shown in Scheme 5.

An alternative approach to the sequence discussed above would be to consider the presence of water in the previous step (addition of imidazole). This corresponds to the mechanism operating via **TS-5a** and **TS-5b** in Scheme 5. Figure 5 shows the 3D models and relative energies of **TS-5a** and **TS-5b** and Table 2 lists the diastereoselectivities calculated for both reaction paths, through **TS-5** and **TS-4**.

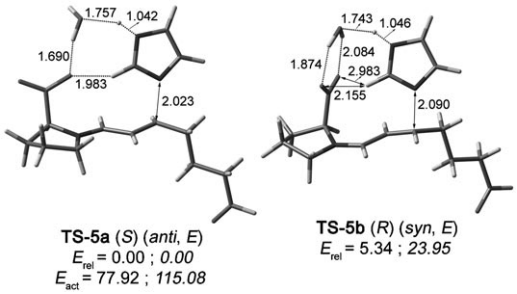

Figure 5. Calculated transition-state structures for the addition of imidazole in the presence of water and the relative gas-phase Gibbs' energies (kJ mol^{-1}) at 0 °C at the B3LYP/6-31G(d,p) (plain text) and PCM B3LYP/6-31++G(d,p)//B3LYP/6-31G(d,p) (*italic*) levels of theory.

Table 2. Relative transition-state energies for the addition of imidazole with or without a molecule of water explicitly considered, yields, and enantioselectivities in the gas phase and in acetonitrile at 0 and 25 °C.[a]

		TS	Gas phase			Acetonitrile	
		ΔG [kJ mol^{-1}]	Yield [%]	*ee* [%]	ΔG [kJ mol^{-1}]	Yield [%]	*ee* [%]
0 °C	**TS-4a** (*S*)	61.12	0.00	79.2 (*S*)	1.66 (−22.31)	33.24	96.2 (*S*)
	TS-5a (*S*)	0.00	89.62		0.00 (37.16)	64.87	
	TS-4b (*R*)	67.15	0.00		8.77 (−21.22)	1.88	
	TS-5b (*R*)	5.34	10.38		23.95 (55.76)	0.00	
25 °C	**TS-4a** (*S*)	57.50	0.00	82.1 (*S*)	0.00 (−22.31)	66.36	92.7 (*S*)
	TS-5a (*S*)	0.00	91.04		1.97 (37.16)	30.00	
	TS-4b (*R*)	63.60	0.00		7.19 (−21.22)	3.64	
	TS-5b (*R*)	5.75	8.96		26.32 (55.76)	0.00	

[a] Gibbs' energy differences are given in brackets: $\Delta\Delta G = \Delta G_{CH3CN} - \Delta G_{GP}$.

The gas-phase activation energy for the addition of imidazole in the presence of water ($E_{act\textbf{TS-5a}} = 77.92$ kJ mol^{-1}) is 61.12 kJ mol^{-1} lower than in anhydrous conditions ($E_{act\textbf{TS-4a}} = 139.04$ kJ mol^{-1}), whereas in solvent the difference is only 1.65 kJ mol^{-1}. These results show that in solvent the two reaction paths have equivalent activation energies and have to be considered when predicting the final reaction selectivity. Thus, in solvent at 0 °C, isomer **6a** results from **TS-4a** and **TS-5a**, whereas isomer **6b** results only from **TS-4b** as **TS-5b** has too high an energy (Scheme 5). Considering the four transitions states, isomer **6a** (*S*) is formed in a yield of 98.1 %, whereas isomer **6b** (*R*) is formed in a yield of 1.9 % (96.2 % *ee*, Table 2). The results discussed above show that the addition of imidazole to the double bond is indeed stereoselective. Nevertheless, the mechanisms discussed here are substantially different from that proposed by Hong and co-workers because the nature of the hydrogen bond is dif-

ferent and because water is an important reagent for the proton transfer between the imidazole ring and the carboxy moiety. Also, according to the proposal of Hong and co-workers, the selectivity results from a preference for attack directed by hydrogen-bond formation, in contrast to a direct attack from the opposite face, without hydrogen-bond formation between the imidazole molecule and the carboxy moiety (Scheme 3). In our model the selectivity results from two possible attacks, both directed by the carboxy group, with or without a water molecule serving as a bridge between the imidazole and the carboxy moieties, but with different orientations of the carbon chain, which allow for different final diastereoselectivities. Even when not present in the transition state, water is always needed for the final proton transfer between the imidazole nitrogen atom and the carboxy group, as was previously discussed.

The next step in the reaction path is the cyclization of the mixture of epimers **6a** and **6b** obtained with an *ee* of 96.2% from the imidazole addition step. The cyclization can occur via eight different transition-state structures, but only four are important in terms of the final stereoselectivity outcome, as shown in Scheme 5 and Figure 6. All four structures have the enamine moiety in the same configuration, but two of them originate from the *S* isomer at the C3 position (**TS-6a** and **TS-6b**) and the other two from the *R* isomer at the C3 position (**TS-6c** and **TS-6d**). Table 3 lists the selectivities predicted on the basis of the initial *S ee* of 96.2% at the C3 position, as previously calculated. The values in Table 3 were calculated assuming that the inverse reaction for the addition of imidazole is slower than the cyclization step, as our PCM results indicate. Thus, the rate-limiting step is the addition of imidazole, which means that compound **6** reacts as soon as it is formed. The final selectivity of the cyclization step is then a result of the selectivity of the imidazole addition step, as well as the selectivity of the cyclization step itself.

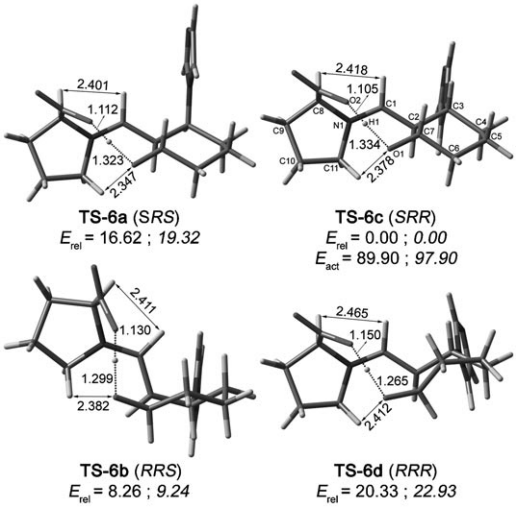

Figure 6. Calculated transition-state structures for the L-proline/imidazole-catalyzed cyclization of **7** to **8** and the relative gas-phase Gibbs' energies (kJ mol^{-1}) at 0°C at the B3LYP/6-31G(d,p) (plain text) and PCM B3LYP/6-31++G(d,p)//B3LYP/6-31G(d,p) (*italic*) levels of theory.

Table 3. Relative transition-state energies, yields, and enantioselectivities of the intramolecular B-H reaction with imidazole as co-catalyst in the gas phase and in acetonitrile at 0 and 25°C.[a]

		TS	Gas phase			Acetonitrile			Ref. [5a]
		ΔG [kJ mol^{-1}]	Yield [%]	*ee* [%]	ΔG [kJ mol^{-1}]	Yield [%]	*ee* [%]	*ee* [%]	
0°C	**TS-6a** (*SRS*)	16.62	2.96	73.3 (*R*)	19.32 (10.70)	1.66	92.9 (*R*)	80[b] (*R*)	
	TS-6b (*RRS*)	8.26	86.66		9.24 (8.99)	96.45			
	TS-6c (*SSR*)	0.00	10.38		0.00 (8.01)	1.89		93[c] (*R*)	
	TS-6d (*RRR*)	20.33	0.00		22.93 (10.61)	0.00			
25°C	**TS-6a** (*SRS*)	16.87	2.86	76.4 (*R*)	19.57 (10.70)	1.55	89.6 (*R*)	59[b] (*R*)	
	TS-6b (*RRS*)	8.38	88.18		9.36 (8.99)	94.79			
	TS-6c (*SRR*)	0.00	8.96		0.00 (8.01)	3.64			
	TS-6d (*RRR*)	20.33	0.00		22.93 (10.61)	0.00			

[a] The selectivities are calculated based on a mixture of epimers **6a** and **6b** with an *ee* of 96.2%. The selectivities are calculated for the final compound **2**. Gibbs' energy differences in brackets: $\Delta\Delta G = \Delta G_{CH_3CN} - \Delta G_{GP}$ At 0°C, $E_{act} = G_{\mathbf{TS\text{-}6c}} - G_{\mathbf{reag}}$; $E_{act} = 89.90$ kJ mol^{-1} in the gas phase and 97.90 kJ mol^{-1} in acetonitrile. At 25°C, $E_{act} = G_{\mathbf{TS\text{-}6c}} - G_{\mathbf{reag}}$; $E_{act} = 96.73$ kJ mol^{-1} in the gas phase and 104.73 kJ mol^{-1} in acetonitrile. [b] 0.1 equivalents of imidazole. [c] 1.0 equivalent of imidazole.

The relative energies in Table 3 and Figure 6 indicate that if the starting material is racemic at the C3 position, then the final product **2** should be nearly racemic, with a slight excess of the *S* isomer. If the starting material has the enantiomeric purity previously calculated for the addition of imidazole (96.2% *S*), as considered in Table 3, then the final product **2** will have the *R* configuration at the newly formed chiral center and an *ee* of 92.9%, in quite good agreement with the experimental result (93%, 0°C). This means that the selectivity of the imidazole addition step is mandatory (**3**→**6**, Scheme 5), as predicted by Hong and co-workers, and has to be the rate-limiting step. Nevertheless, the imidazole addition has to be faster than the imine/enamine conversion (**3**→**4**, Scheme 4) because this step leads to the opposite final configuration.

The transition-state structures in Figure 6 are similar to those in Figure 3 because the major electrostatic factors conditioning the geometries and energies are similar. Nevertheless, the presence of the imidazole ring introduces a new factor, which has to be considered as it can be in either an equatorial or axial orientation, which results in substantial differences in the calculated activation energies.

The imidazole ring is in an equatorial position for all the structures, with the exception of **TS-6a**. Structure **TS-6a** is very similar to structure **TS-6c**, but is 16.6 kJ mol^{-1} less stable (Figure 6, gas phase). In **TS-6a** the contact distance between O1 and C11H is shorter than in **TS-6c** and, as a

consequence, the energy of the first structure should be lower ($d_{C11H-O1}=2.347$ Å in **TS-6a** and $d_{C11H-O1}=2.378$ Å in **TS-6c**). However, this effect is counterbalanced by the axial (**TS-6a**) versus equatorial (**TS-6c**) orientations of the imidazole ring, such that **TS-6c** is in fact the most stable transition-state structure. Structure **TS-6d** should be identical to structure **TS-6b**, differing only in the relative orientations of the imidazole ring. However, the imidazole moiety prefers to be, in both cases, in the equatorial position, which results in a distortion of the ideal chair conformation of the forming ring in structure **TS-6d**. This structure adopts a boat conformation and, as a result, its gas-phase energy is 20.3 kJ mol^{-1} higher than the energy of **TS-6c**. The larger contact distance between O1 and C11H ($d_{C11H-O1}=2.412$ Å in **TS-6d**), imposed by the distortion of the forming ring, also contributes to this value, and is of major importance for the stabilization of all transition-state structures, as was previously discussed.

Hong and co-workers reported that the reaction selectivity depends not only on solvent polarity, but also on the temperature, because at a lower temperature (0 °C) the selectivity is greater than at 25 °C. Table 3 shows the selectivities calculated for the B–H cyclization reaction after the addition of imidazole at both temperatures, based on an initial mixture of **6a** and **6b** with an *ee* of 96.2%, and indeed shows that the selectivity increases when the temperature is lowered. Nevertheless, a comparison of the relative energy values in Table 3 indicate that the selectivity of the cyclization step is not strongly dependent on the temperature, which means that the calculated final selectivity must depend on the imidazole addition step (Table 2). A comparison of the energy values in Table 2 for each individual reaction path also shows that none of them accounts for any selectivity dependence on temperature. However, the two addition paths together indeed show a dependence on selectivity with temperature. As the path with water included is more sensitive to temperature, at lower temperatures it accounts to a larger extent for the selectivity (**TS-5a**), whereas at higher temperatures the anhydrous path is preferred (**TS-4a**). The averaged result predicts better selectivity at lower temperatures, in accord with the results observed experimentally.

In spite of the energy relations discussed above that can justify the experimental observations of selectivity dependence on temperature, other factors can also contribute. We have already shown that the addition of imidazole is less energetic than the imine/enamine conversion, whether it be the direct or water-catalyzed conversion (Schemes 4 and 5). However, in the presence of imidazole, another mechanism can be proposed for the imine/enamine conversion in which imidazole is substituted for water as the catalyst, as in Scheme 6 and Figure 7. If imidazole can substantially reduce the activation energy of the imine/enamine conversion step, then this step can compete with the addition of imidazole and thus lead to a reduction of the selectivity. In addition, if the imidazole-catalyzed imine/enamine conversion shows a strong energy dependence on temperature, it could also account for the observed selectivity dependence on temperature.

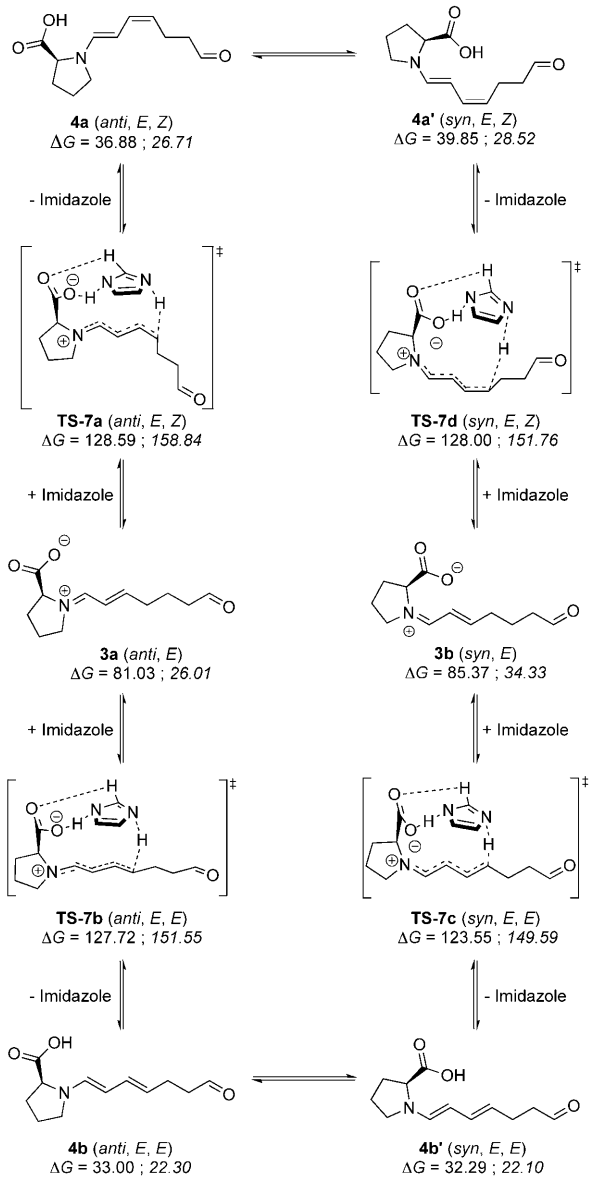

Scheme 6. Proposed imidazole-catalyzed path for the imine/enamine conversion. Free energies (kJ mol^{-1}) calculated at 0 °C at the B3LYP/6-31G(d,p) (plain text) and PCM B3LYP/6-31++G(d,p)//B3LYP/6-31G(d,p) (*italic*) levels of theory.

Table 4 compares the relative energies and selectivities obtained for the formation of enamine catalyzed by water or imidazole. The overall conclusion is that imidazole indeed seems to be a better catalyst for the imine/enamine conversion as it reduces the activation energy by about 21 kJ mol^{-1} ($\Delta G_{\mathbf{TS\text{-}2d}}-\Delta G_{\mathbf{TS\text{-}7d}}$ at 0 °C). At the same time, although water mainly catalyzes the formation of **4b′** (99%, Scheme 4), a compound that is not active in the following cyclization step, imidazole catalyzes the formation of **4a** and **4a′** to give a yield of around 25% (Scheme 6, Table 4 (yield of **TS-7a** + yield of **TS-7d**)). In spite of these results, the im-

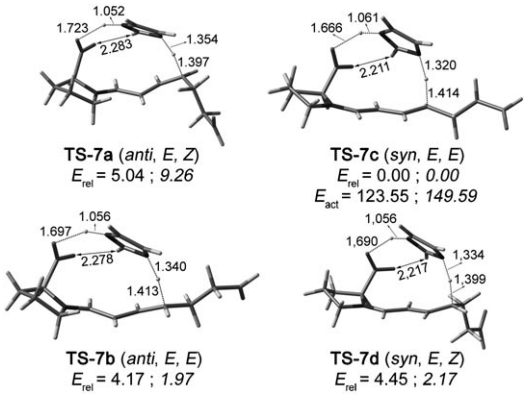

Figure 7. Calculated transition-state structures for the imidazole-catalyzed imine/enamine conversion and the relative gas phase Gibbs' energies (kJ mol^{-1}) at 0 °C at the B3LYP/6-31G(d,p) (plain text) and PCM B3LYP/6-31++G(d,p)//B3LYP/6-31G(d,p) (*italic*) levels of theory.

idazole addition step (**TS-5a**, Scheme 5) is still around 37 kJ mol^{-1} less energetic than the imidazole-catalyzed imine/enamine formation step (**TS-7d**, Scheme 6). This indicates that, when the two possible paths are considered, the imine/enamine conversion step outlined in Scheme 6 does not occur concurrently with the imidazole addition step (Scheme 5) and that the dependence of selectivity on temperature has to result from the imidazole addition step, as discussed before.

Recently[22b] we discussed the effect of water on the stereoselectivity of L-proline-catalyzed intramolecular aldol reactions of dialdehydes. According to our results, in the presence of water the enantio- and diastereoselectivity of this type of reaction decrease. Nevertheless, we also concluded that if solvent effects are considered, the activation energies of transition-state structures with a water molecule explicitly included are substantially higher than those of transition-state structures free of water.

As we previously suggested that water is of major importance in the imidazole addition step and in the imine/enamine conversion step (in the absence of imidazole), we also decided to test its eventual importance in the cyclization step. The results shown in Table 5 and Figure 8 are interesting as they predict that if water is included then both configurations of the imidazole would induce the formation of *R* as the final configuration of the newly formed chiral center. This dramatic change is mainly a result of the strong reduction in the activation energy of **TS-8d**, relative to **TS-6d** (Figure 8 and Figure 6). The presence of water allows the formation of several electrostatic contacts, which compensate the loss of contact between O1 and C11H. This permits

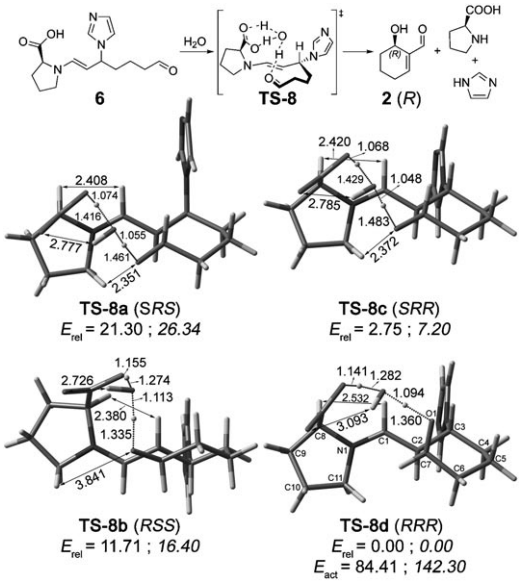

Figure 8. Calculated transition-state structures for the L-proline/imidazole-catalyzed cyclization of **7** to **8** in the presence of water and the relative gas-phase Gibbs' energies (kJ mol^{-1}) at 0 °C at the B3LYP/6-31G(d,p) (plain text) and PCM B3LYP/6-31++G(d,p)//B3LYP/6-31G(d,p) (*italic*) levels of theory.

Table 4. Comparison of the relative free energies and yields of the imine/enamine conversion catalyzed by water (**TS-2**) or imidazole (**TS-7**) at 0 and 25 °C.[a]

	TS	Gas phase				Acetonitrile			
		TS-2		**TS-7**		**TS-2**		**TS-7**	
		ΔG [kJ mol^{-1}]	Yield [%]	ΔG [kJ mol^{-1}]	Yield [%]	ΔG [kJ mol^{-1}]	Yield [%]	ΔG [kJ mol^{-1}]	Yield [%]
0 °C	**TS-a** (*anti*,*E*,*Z*)	30.58	0.00	5.04	8.82	17.41 (23.06)	0.08	9.26 (23.76)	1.26
	TS-b (*anti*,*E*,*E*)	26.54	0.00	4.17	12.54	14.18 (23.87)	0.31	1.97 (23.83)	23.91
	TS-c (*syn*,*E*,*E*)	0.00	93.79	0.00	67.45	0.00 (36.23)	93.41	0.00 (26.04)	52.83
	TS-d (*syn*,*E*,*Z*)	6.73	6.21	4.45	11.20	6.73 (36.22)	6.20	2.17 (23.76)	23.91
25 °C	**TS-a** (*anti*,*E*,*Z*)	30.26	0.00	5.01	8.87	17.09 (23.06)	0.10	9.23 (23.76)	1.27
	TS-b (*anti*,*E*,*E*)	26.28	0.00	4.13	12.67	13.92 (23.87)	0.34	1.93 (23.83)	24.08
	TS-c (*syn*,*E*,*E*)	0.00	94.13	0.00	67.07	0.00 (36.23)	93.71	0.00 (26.04)	52.36
	TS-d (*syn*,*E*,*Z*)	6.88	5.87	4.40	11.39	6.87 (36.22)	5.85	2.12 (23.76)	22.29

[a] Gibbs' energy differences in brackets: $\Delta\Delta G = \Delta G_{CH_3CN} - \Delta G_{GP}$. With water at 0 °C, $E_{act} = G_{\mathbf{TS\text{-}2c}} - G_{\mathbf{reag}}$; $E_{act} = 129.58$ kJ mol^{-1} in the gas phase and 165.81 kJ mol^{-1} in acetonitrile. With water at 25 °C, $E_{act} = G_{\mathbf{TS\text{-}2c}} - G_{\mathbf{reag}}$; $E_{act} = 134.87$ kJ mol^{-1} in the gas phase and 171.10 kJ mol^{-1} in acetonitrile. With imidazole at 0 °C, $E_{act} = G_{\mathbf{TS\text{-}7c}} - G_{\mathbf{reag}}$; $E_{act} = 123.55$ kJ mol^{-1} in the gas phase and 149.59 kJ mol^{-1} in acetonitrile. With imidazole at 25 °C, $E_{act} = G_{\mathbf{TS\text{-}7c}} - G_{\mathbf{reag}}$; $E_{act} = 129.27$ kJ mol^{-1} in the gas phase and 155.31 kJ mol^{-1} in acetonitrile.

Table 5. Relative transition-state energies, yields, and enantioselectivities of the intramolecular B–H reaction with imidazole as co-catalyst and a molecule of water explicitly considered in the gas phase and acetonitrile at 0 °C.[a]

TS	Gas phase			Acetonitrile			Ref. [5a]
	ΔG [kJ mol^{-1}]	Yield [%]	*ee* [%]	ΔG [kJ mol^{-1}]	Yield [%]	*ee* [%]	*ee* [%]
TS-8a (*SRS*)	21.30	1.83	91.2 (*R*)	26.34 (62.93)	1.75	96.3 (*R*)	80[b] (*R*)
TS-8b (*RSS*)	11.71	87.79		16.40 (62.59)	96.36		
TS-8c (*SRR*)	2.75	2.57		7.20 (62.34)	0.10		93[c] (*R*)
TS-8d (*RRR*)	0.00	7.81		0.00 (57.89)	1.79		

[a] With water at 0 °C, $E_{act} = G_{\mathbf{TS\text{-}8d}} - G_{\mathbf{reag}}$; $E_{act} = 84.41$ kJ mol^{-1} in the gas phase and 142.30 kJ mol^{-1} in acetonitrile. [b] 0.1 equivalents of imidazole. [c] 1.0 equivalent of imidazole.

the forming ring in **TS-8d** to adopt a chair conformation with the carbonyl group in an axial position and the imidazole ring in an equatorial orientation. The absolute configuration of the structure **TS-8b** (*RSS*) is now different to the absolute configuration of the structure **TS-6b** (*RRS*). Nevertheless, as the relative energies of the structures **TS-8a** and **TS-8b** are similar to those calculated for **TS-6a** and **TS-6b**, the predicted final selectivity is the *R* configuration at the C3 position, as is experimentally observed. In spite of this interesting result, the inclusion of solvent effects substantially increases the activation energies of all the transition states, which suggests, as reported in our previous paper, that water is not present during the cyclization step.

Conclusion

The mechanisms proposed by Hong and co-workers for the intramolecular Baylis–Hillman reaction of hept-2-enedial catalyzed by (*S*)-proline have been analyzed by using the B3LYP/6-31G(d,p) and PCM B3LYP/6-31G++(d,p)//B3LYP/6-31G(d,p) theoretical models. The data obtained allow the rationalization of the main factors that contribute to the selectivity of the reaction in the absence of imidazole as co-catalyst as well as the observed improvement in selectivity and inversion of configuration when imidazole is present in the reaction medium. The theoretical data obtained with the PCM model using acetonitrile as solvent essentially agree with the experimental results of Hong and co-workers. Water was found to be an important reagent, acting as a catalyst in the imine/enamine conversion step, when imidazole is not present. When imidazole is used as co-catalyst, water is also very important to catalyze the proton transfer between the imidazole ring and the proline carboxy group. Proline is important as a selectivity inductor in two different reaction steps, the cyclization and the addition of imidazole. The selectivity of the cyclization step, in the absence or in the presence of imidazole, mainly results from important electrostatic contacts between the carbonyl oxygen atom and the proline moiety. These contacts are, in many aspects, similar to those found in the proline-catalyzed intramolecular aldol reactions of 1,7-dialdehydes. The selectivity observed in the imidazole addition step mainly results from the two possible conformations of the carbon chain in relation to the carbonyl group in the proline moiety as the addition reaction does not occur if hydrogen-bonding between the imidazole ring and the carboxy group is not established. The overall selectivity of the reaction is a result of the selectivities calculated for the imidazole addition and cyclization steps.

Computational Methods

All calculations were performed by using density functional theory[26] with the Gaussian 03 software package.[27] The geometries of all stationary points were full optimized with the B3LYP/6-31G(d,p) functional and their nature (minimum or transition state) was determined by frequency analysis. Zero-point energies and thermal corrections have been taken from unscaled vibrational frequencies. Reported activation energies include zero-point corrections. The effect of solvent on the energies was studied by single-point calculations at the B3LYP/6-31++G(d,p)//B3LYP/6-31G(d,p) level of theory. The polarizable continuum model (PCM)[28] was used together with UAKS radii and the dielectric constant of acetonitrile (CH_3CN). All bond lengths are given in angstroms (Å), angles in degrees, and energy values in kJ mol^{-1}. Activation energies are calculated relative to the reagents.

Acknowledgement

We are grateful to the Fundação para a Ciência e Tecnologia (SFRH/BD/17547/2004) for financial support.

[1] a) A. Berkessel, H. Gröger, *Asymmetric Organocatalysis: From Biomimetic Concepts to Applications in Asymmetric Synthesis*, Wiley, New York, **2005**; b) W. Notz, F. Tanaka, C. F. Barbas, *Acc. Chem. Res.* **2004**, *37*, 580–591; c) A. Berkessel, *Pure Appl. Chem.* **2005**, *77*, 1277–1284; d) J. Seayad, B. List, *Org. Biomol. Chem.* **2005**, *3*, 719–724; e) P. I. Dalko, L. Moisan, *Angew. Chem.* **2004**, *116*, 5248–5286; *Angew. Chem. Int. Ed.* **2004**, *43*, 5138–5175; f) A. M. Rouhi, *Chem. Eng. News* **2004**, *82*, 41–45.

[2] a) B. List, *J. Am. Chem. Soc.* **2000**, *122*, 9336–9337; b) N. S. Chowdari, J. T. Suri, C. F. Barbas, *Org. Lett.* **2004**, *6*, 2507–2510; c) T. Kano, Y. Yamaguchi, O. Tokuda, K. Maruoka, *J. Am. Chem. Soc.* **2005**, *127*, 16408–16409; d) S. Mitsumori, H. Zhang, P. H. Y. Cheong, K. N. Houk, F. Tanaka, C. F. Barbas, *J. Am. Chem. Soc.* **2006**, *128*, 1040–1041.

[3] a) O. Andrey, A. Alexakis, G. Bernardinelli, *Org. Lett.* **2003**, *5*, 2559–2561; b) M. T. H. Fonseca, B. List, *Angew. Chem.* **2004**, *116*, 4048–4050; *Angew. Chem. Int. Ed.* **2004**, *43*, 3958–3960; c) N. Mase, R. Thayumanavan, F. Tanaka, C. F. Barbas, *Org. Lett.* **2004**, *6*, 2527–2530.

[4] a) A. B. Northrup, D. W. C. MacMillan, *J. Am. Chem. Soc.* **2002**, *124*, 6798–6799; b) K. Sakthivel, W. Notz, T. Bui, C. F. Barbas, *J. Am. Chem. Soc.* **2001**, *123*, 5260–5267; c) C. Allemann, R. Gordillo, F. R. Clemente, P. H. Y. Cheong, K. N. Houk, *Acc. Chem. Res.* **2004**, *37*, 558–569; d) C. Pidathala, L. Hoang, N. Vignola, B. List, *Angew. Chem.* **2003**, *115*, 2891–2894; *Angew. Chem. Int. Ed.* **2003**, *42*, 2785–2788.

[5] a) S. H. Chen, B. C. Hong, C. F. Su, S. Sarshar, *Tetrahedron Lett.* **2005**, *46*, 8899–8903; b) D. Basavaiah, A. J. Rao, T. Satyanarayana,

Chem. Rev. **2003**, *103*, 811–891; c) D. Basavaiah, K. V. Rao, R. J. Reddy, *Chem. Soc. Rev.* **2007**, *36*, 1581–1588.
[6] a) A. B. Northrup, D. W. C. MacMillan, *J. Am. Chem. Soc.* **2002**, *124*, 2458–2460; b) D. B. Ramachary, N. S. Chowdari, C. F. Barbas, *Angew. Chem.* **2003**, *115*, 4365–4369; *Angew. Chem. Int. Ed.* **2003**, *42*, 4233–4237; c) K. Juhl, K. A. Jorgensen, *Angew. Chem.* **2003**, *115*, 1536–1539; *Angew. Chem. Int. Ed.* **2003**, *42*, 1498–1501.
[7] a) A. Bogevig, K. Juhl, N. Kumaragurubaran, W. Zhuang, K. A. Jorgensen, *Angew. Chem.* **2002**, *114*, 1868–1871; *Angew. Chem. Int. Ed.* **2002**, *41*, 1790–1793; b) N. Kumaragurubaran, K. Juhl, W. Zhuang, A. Bogevig, K. A. Jorgensen, *J. Am. Chem. Soc.* **2002**, *124*, 6254–6255; c) B. List, *J. Am. Chem. Soc.* **2002**, *124*, 5656–5657; d) N. S. Chowdari, C. F. Barbas, *Org. Lett.* **2005**, *7*, 867–870; e) J. T. Suri, D. D. Steiner, C. F. Barbas, *Org. Lett.* **2005**, *7*, 3885–3888.
[8] N. Vignola, B. List, *J. Am. Chem. Soc.* **2004**, *126*, 450–451.
[9] a) M. P. Sibi, M. Hasegawa, *J. Am. Chem. Soc.* **2007**, *129*, 4124–4125; b) M. Engqvist, J. Casas, H. Sunden, I. Ibrahem, A. Cordova, *Tetrahedron Lett.* **2005**, *46*, 2053–2057.
[10] a) S. Mayer, B. List, *Angew. Chem.* **2006**, *118*, 4299–4301; *Angew. Chem. Int. Ed.* **2006**, *45*, 4193–4195; b) S. G. Ouellet, J. B. Tuttle, D. W. C. MacMillan, *J. Am. Chem. Soc.* **2005**, *127*, 32–33.
[11] a) S. Brandau, E. Maerten, K. A. Jorgensen, *J. Am. Chem. Soc.* **2006**, *128*, 14986–14991; b) R. Rios, H. Sunden, I. Ibrahem, G. L. Zhao, L. Eriksson, A. Cordova, *Tetrahedron Lett.* **2006**, *47*, 8547–8551; c) M. Marigo, T. Schulte, J. Franzen, K. A. Jorgensen, *J. Am. Chem. Soc.* **2005**, *127*, 15710–15711.
[12] a) I. Ibrahem, R. Rios, J. Vesely, G. L. Zhao, A. Cordova, *Chem. Commun.* **2007**, 849–851; b) J. Vesely, I. Ibrahem, G. L. Zhao, R. Rios, A. Cordova, *Angew. Chem.* **2007**, *119*, 792–795; *Angew. Chem. Int. Ed.* **2007**, *46*, 778–781.
[13] S. Bertelsen, P. Diner, R. L. Johansen, K. A. Jorgensen, *J. Am. Chem. Soc.* **2007**, *129*, 1536–1537.
[14] a) H. Gotoh, R. Masui, H. Ogino, M. Shoji, Y. Hayashi, *Angew. Chem.* **2006**, *118*, 7007–7010; *Angew. Chem. Int. Ed.* **2006**, *45*, 6853–6856; b) S. Brandau, A. Landa, J. Franzen, M. Marigo, K. A. Jorgensen, *Angew. Chem.* **2006**, *118*, 4411–4415; *Angew. Chem. Int. Ed.* **2006**, *45*, 4305–4309; c) K. A. Ahrendt, C. J. Borths, D. W. C. MacMillan, *J. Am. Chem. Soc.* **2000**, *122*, 4243–4244.
[15] a) J. Jauch, *Angew. Chem.* **2000**, *112*, 2874–2875; *Angew. Chem. Int. Ed.* **2000**, *39*, 2764–2765; b) J. Jauch, *Eur. J. Org. Chem.* **2001**, 473–476; c) C. R. Mateus, M. P. Feltrin, A. M. Costa, F. Coelho, W. P. Almeida, *Tetrahedron* **2001**, *57*, 6901–6908; d) B. M. Trost, O. R. Thiel, H. C. Tsui, *J. Am. Chem. Soc.* **2002**, *124*, 11616–11617; e) W. P. Almeida, F. Coelho, *Tetrahedron Lett.* **2003**, *44*, 937–940; f) B. M. Trost, O. R. Thiel, H. C. Tsui, *J. Am. Chem. Soc.* **2003**, *125*, 13155–13164; g) P. R. Krishna, M. Narsingam, V. Kannan, *Tetrahedron Lett.* **2004**, *45*, 4773–4775; h) D. J. Mergott, S. A. Frank, W. R. Roush, *Proc. Natl. Acad. Sci. USA* **2004**, *101*, 11955–11959.
[16] a) M. L. Bode, P. T. Kaye, *Tetrahedron Lett.* **1991**, *32*, 5611–5614; b) K. E. Price, S. J. Broadwater, H. M. Jung, D. T. McQuade, *Org. Lett.* **2005**, *7*, 147–150; c) V. K. Aggarwal, S. Y. Fulford, G. C. Lloyd-Jones, *Angew. Chem.* **2005**, *117*, 1734–1736; *Angew. Chem. Int. Ed.* **2005**, *44*, 1706–1708; d) R. Robiette, V. K. Aggarwal, J. N. Harvey, *J. Am. Chem. Soc.* **2007**, *129*, 15513–15525; e) D. Roy, R. B. Sunoj, *Org. Lett.* **2007**, *9*, 4873–4876; f) J. Xu, *THEOCHEM* **2006**, *767*, 61–66.
[17] a) G. E. Keck, D. S. Welch, *Org. Lett.* **2002**, *4*, 3687–3690; b) K. Yagi, T. Turitani, H. Shinokubo, K. Oshima, *Org. Lett.* **2002**, *4*, 3111–3114; c) E. L. Richards, P. J. Murphy, F. Dinon, S. Fratucello, P. M. Brown, T. Gelbrich, M. B. Hursthouse, *Tetrahedron* **2001**, *57*, 7771–7784; d) F. Dinon, E. Richards, P. J. Murphy, D. E. Hibbs, M. B. Hursthouse, K. M. Abdul Malik, *Tetrahedron Lett.* **1999**, *40*, 3279–3282; e) G. P. Black, F. Dinon, S. Fratucello, P. J. Murphy, M. Nielsen, H. L. Williams, *Tetrahedron Lett.* **1997**, *38*, 8561–8564.
[18] a) C. E. Aroyan, M. M. Vasbinder, S. J. Miller, *Org. Lett.* **2005**, *7*, 3849–3851; b) M. E. Krafft, T. F. N. Haxell, K. A. Seibert, K. A. Abboud, *J. Am. Chem. Soc.* **2006**, *128*, 4174–4175; c) R. R. Huddleston, M. J. Krische, *Synlett* **2003**, 12–21; d) M. E. Krafft, J. A. Wright, *Chem. Commun.* **2006**, 2977–2979; e) W. D. Teng, R. Huang, C. K. W. Kwong, M. Shi, P. H. Toy, *J. Org. Chem.* **2006**, *71*, 368–371.
[19] a) P. Langer, *Angew. Chem.* **2000**, *112*, 3177–3180; *Angew. Chem. Int. Ed.* **2000**, *39*, 3049–3052; b) E. Ciganek, *Organic Reactions, Vol. 51*, Wiley, New York, **1997**; c) D. Basavaiah, P. D. Rao, R. S. Hyma, *Tetrahedron* **1996**, *52*, 8001–8062; d) S. E. Drewes, G. H. P. Roos, *Tetrahedron* **1988**, *44*, 4653–4670; e) A. B. Baylis, M. E. D. Hillman, German Patent 2155113, **1972**; [*Chem. Abstr.* **1972**, 34174].
[20] M. Shi, J.-K. Jiang, C.-Q. Li, *Tetrahedron Lett.* **2002**, *43*, 127–130.
[21] F. R. Clemente, K. N. Houk, *Angew. Chem.* **2004**, *116*, 5890–5892; *Angew. Chem. Int. Ed.* **2004**, *43*, 5766–5768.
[22] a) S. Bertelsen, M. Marigo, S. Brandes, P. Diner, K. A. Jorgensen, *J. Am. Chem. Soc.* **2006**, *128*, 12973–12980; b) F. J. S. Duarte, E. J. Cabrita, G. Frenking, A. G. Santos, *Eur. J. Org. Chem.* **2008**, *2008*, 3397–3402.
[23] a) D. J. Hupe, M. C. R. Kendall, T. A. Spencer, *J. Am. Chem. Soc.* **1972**, *94*, 1254–1263; b) R. D. Roberts, H. E. Ferran, M. J. Gula, T. A. Spencer, *J. Am. Chem. Soc.* **1980**, *102*, 7054–7058.
[24] F. R. Clemente, K. N. Houk, *J. Am. Chem. Soc.* **2005**, *127*, 11294–11302.
[25] C. E. Cannizzaro, K. N. Houk, *J. Am. Chem. Soc.* **2002**, *124*, 7163–7169.
[26] R. G. Y. Parr, W. Yang, *Density Functional Theory of Atoms and Molecules*, Oxford University Press, Oxford, **1989**.
[27] Gaussian 03, Revision E.01, M. J. Frisch, G. W. Trucks, H. B. Schlegel, G. E. Scuseria, M. A. Robb, J. R. Cheeseman, J. A. Montgomery, Jr., T. Vreven, K. N. Kudin, J. C. Burant, J. M. Millam, S. S. Iyengar, J. Tomasi, V. Barone, B. Mennucci, M. Cossi, G. Scalmani, N. Rega, G. A. Petersson, H. Nakatsuji, M. Hada, M. Ehara, K. Toyota, R. Fukuda, J. Hasegawa, M. Ishida, T. Nakajima, Y. Honda, O. Kitao, H. Nakai, M. Klene, X. Li, J. E. Knox, H. P. Hratchian, J. B. Cross, V. Bakken, C. Adamo, J. Jaramillo, R. Gomperts, R. E. Stratmann, O. Yazyev, A. J. Austin, R. Cammi, C. Pomelli, J. W. Ochterski, P. Y. Ayala, K. Morokuma, G. A. Voth, P. Salvador, J. J. Dannenberg, V. G. Zakrzewski, S. Dapprich, A. D. Daniels, M. C. Strain, O. Farkas, D. K. Malick, A. D. Rabuck, K. Raghavachari, J. B. Foresman, J. V. Ortiz, Q. Cui, A. G. Baboul, S. Clifford, J. Cioslowski, B. B. Stefanov, G. Liu, A. Liashenko, P. Piskorz, I. Komaromi, R. L. Martin, D. J. Fox, T. Keith, M. A. Al-Laham, C. Y. Peng, A. Nanayakkara, M. Challacombe, P. M. W. Gill, B. Johnson, W. Chen, M. W. Wong, C. Gonzalez, J. A. Pople, Gaussian, Inc., Wallingford, CT, **2004**.
[28] M. Cossi, G. Scalmani, N. Rega, V. Barone, *J. Chem. Phys.* **2002**, *117*, 43–54.

Received: June 9, 2008
Revised: October 26, 2008
Published online: January 2, 2009

